Exploitation of drainage water heat: A novel solution experimented at the Brenner Base Tunnel

F. Tinti [a,*], C. Spaggiari [b], M. Lanconelli [c], A. Voza [c], D. Boldini [d]

[a] Department of Civil, Chemical, Environmental and Materials Engineering, University of Bologna, via Terracini 28, 40121 Bologna, Italy
[b] Department of Structural and Geotechnical Engineering, Sapienza University of Rome, Via Eudossiana 18, 00184 Roma, Italy
[c] BBT Brenner Base Tunnel BBT SE, Piazza Stazione 1, I-39100 Bolzano, Italy
[d] Department of Chemical Engineering Materials Environment, Sapienza University of Rome, Via Eudossiana 18, 00184 Roma, Italy

ABSTRACT

Deep tunnels in permeable fractured rock-masses and under high piezometric levels can drain notable volumes of warm water, which are collected under gravity in specific conduits towards the portals, where heat can be exploited. The utilization of this energy source is generally narrowed by the limited presence of end-users near the portals, while other promising heating and cooling needs can be found directly along the tunnel length. The work presents the design, construction and installation of a geothermal system prototype exploiting the drainage water heat directly inside the tunnel. The prototype was named Smart Flowing due to the peculiarity of its heat exchange process. The system was realized and installed inside the exploratory tunnel of the Brenner Base Tunnel, near the border between Italy and Austria. The Smart Flowing modules were built outside and later moved inside the tunnel, where they were placed and assembled concurrently to the advancement of the Tunnel Boring Machine. A design procedure was proposed and validated against a testing and monitoring campaign. The data from the experimental activity confirmed that the drainage water flow guarantees long-term stabilization of circulating water temperature and fast heat recovery afterwards, thus securing the considerable power and performance values of a water-water heat pump connected to the system. A sensitivity analysis allowed the reproduction of different working scenarios, in order to generalize the application of Smart Flowing beyond the specific installation context.

1. Introduction

1.1. Geothermal energy exploitation in tunnels

Deep tunnels may drain large volumes of warm water in permeable fractured rock-masses and under high piezometric levels. Generally, the water inflows are collected and drained away under gravity in specific conduits, from the point of maximum elevation towards the portals. Their flow rate and temperature depend on the natural inflow conditions, but also on the drainage system design. Once out of the tunnel, the water is typically cooled in dedicated treatment plants. Afterwards, it is discharged into rivers at temperatures and flow rates regulated by environmental protection standards, usually limiting the tunnel water uptake. In many locations, cooling ponds and/or towers are necessary to decrease water temperatures prior to its disposal.

More recently, heat recovery from tunnel drained water has been carried out directly at the portals. This happens for a dual purpose: to respect the environment and to sustainably exploit the drainage water heat. The usable power is mainly governed by the water temperature levels and the steady-state inflows; therefore, its use is commonly guaranteed through connection with heat pump (HP) systems (Stemmle et al., 2022).

In the Alpine context, the thermal use of drainage water from tunnel infrastructures is an already widely implemented technique. The most notable examples are the Gotthard highway tunnel, the Furka railway tunnel, the Ricken railway tunnel, the Mappo-Morettina highway tunnel, the Hauenstein railway tunnel and the Lotschberg base tunnel (Rybach, 2010). In-depth research into tunnel water exploitation at the portals for heating purposes is currently underway at the Gotthard base tunnel (Rybach and Busslinger, 2013) and at the Brenner Base Tunnel (BBT), on both sides of the Italy/Austria border (Kostner, 2011; Casale et al. 2015; Burger et al., 2022; Geisler et al., 2022); in addition, a

preliminary feasibility study was developed at the Lyon-Turin base tunnel for the Maddalena exploratory tunnel (Dematteis et al., 2016).

The already existing applications, all located in Switzerland, are summarised by Wilhelm and Rybach (2003).

The oldest installation for the utilization of tunnel water heat is at the Gotthard highway tunnel and has been in operation since 1979. The outflow rate at the south portal is about 110 l/s with a temperature of 17 °C. A heat pump supplies a highway service centre, while the water is cooled down to 2.3 °C.

The use of underground water at the Furka railway tunnel, in service since 1991, is an example of district heating system with decentralized heat pumps. The tunnel water discharge, characterised by a flow rate of 90 l/s and a 16 °C temperature, is piped to individual houses in the nearby village of Obernwald. There, a network of single heat pumps serves for the double purpose of temperature increase and cooling down the tunnel water.

Located at the south portal of the Ricken railway tunnel, several buildings and facilities in Kaltbrunn have been heated by tunnel water using a HP system since 1998. The outflow rate of the tunnel water is 12 l/s, with a temperature of 12 °C.

The water discharge at the northern portal of the Mappo-Morettina highway tunnel is 16 l/s, with a temperature of 16 °C, and has been used for space heating of the nearby sport and recreation centre since 1999.

150 apartments in Trimbach have been heated and supplied with domestic hot water by the underground water coming from the Hauenstein railway tunnel since 1999. The discharge rate at the south portal is 42 l/s at a temperature of 19 °C.

An innovative project for the exploitation of underground water heat coming from the northern portal of the Lotschberg base tunnel is the Frutigen Tropical House. A cascade use for the heat is applied: firstly, drainage water at 17 °C provides heat to a greenhouse, where tropical plants are grown and Tilapia fish are bred; then, the cooled tunnel water is reused for the breeding of sturgeons and Rainbow trout in outdoor basins at 12 to 15 °C; finally, the tunnel water is further cooled down in an equalizing reservoir, from where it is piped into the Kander river (Rybach, 2015).

Despite these examples, tunnel heat utilisation is generally narrowed by a limited presence of potential end-users and facilities close to the exploitation areas. In this respect, the implementation of modern district heating and cooling grids with decentralized heat pumps could be an efficient solution, since fluid can cover long distances without significant heat losses (Meibodi and Loveridge, 2022). However, in many deep tunnel systems the portals are simply too far from any possible consumer, while other accesses may be in more promising positions, where villages and facilities are present. The application of a system exchanging heat with tunnels could be a further benefit for the inhabitants affected by the tunnel construction. Furthermore, the use of drainage water energy potential along the tunnel length would untap new possibilities, especially if located in more convenient sites rather than at the portals. Currently these implementations are at the initial stage and mainly developed for city tunnels (Frodl et al., 2010; Buhmann et al., 2016; Insana and Barla, 2020). For instance, the emergency stations inside the tunnel could benefit from temperature control, provided by heat exchange with the drainage water temperature.

Heat exploitation along the tunnel length is a challenging task that is closely linked to the tunnel design. It can be obtained by building specific heat exchangers, inserted in the invert elements or in the lining. However, their installation must be compatible with the tunnel advancement and should not slow down the operations. A prototype with these features has been installed in the exploratory tunnel of the BBT system. It was designed and devised thanks to the long-lasting collaboration on geothermal energy topics between the company BBT SE and the University of Bologna (Boldini et al., 2016; Boldini et al., 2018; Foderà et al., 2020; Voza et al., 2022). The prototype concept, named "Smart Flowing", was installed in the tunnel in November 2020

and is fully described by Spaggiari et al. (2022).

The present paper outlines the results of the monitoring campaign for thermal exploitation of the drainage water heat that is in contact with the prototype.

The monitoring campaign aimed to extrapolate general considerations for proper modelling of the Smart Flowing (SF) system and for the further extension of the concept to tunnels at various locations, and of different shapes and dimensions. Therefore, the final purpose was the formulation of a general model to possibly expand its application in the future.

In the following, the main results of the tests are presented together with a dynamic evaluation of the potential heat exploitation. The impact of variations in the drainage water flow conditions on the performance of the prototype was assessed by a sensitivity analysis, which provided a realistic range of temperatures for the most suitable application of Smart Flowing in different mountain tunnel environments. The paper is integrated by a preliminary economic analysis based on the actual costs of prototype installation.

1.2. The Brenner Base tunnel system and geothermal energy

The Brenner Base Tunnel is a 55 km long railway base tunnel excavated through the Eastern Alps connecting the village of Fortezza (Italy) with the city of Innsbruck (Austria). The complex tunnel network has an overall length of over 230 km, which comprises an exploratory tunnel and two main tunnel tubes, in addition to cross passages, emergency stations and access tunnels. On the Italian side, there are also two service tunnel portals: Aica, where drainage water is conveyed, and Mules, a lateral access tunnel (Fig. 1).

With the growing interest in energy exploitation from tunnels, the BBT system has soon become the focus of interest for various geothermal studies. A preliminary investigation of the possible direct use of drainage water collected at the Aica portal took place in 2011 (Kostner, 2011), while in 2015 three further analyses were developed within the SWIFTLY GREEN - Sweden-Italy Freight Transport and Logistics Green Corridor - project (Casale et al., 2015). They focussed on:

- the estimation and mapping of mountain rock temperature at different depths;
- the quantification of the thermal energy of drainage water at the Aica portal;
- the assessment of the potential for energy tunnel lining installation at various tunnel sections.

On the Italian side of the BBT system, two different sites were specifically investigated in terms of potential end-users:

- the Aica service tunnel portal, 2.3 km south of the village of Fortezza with a sparse population of 1078 inhabitants (ISTAT, Fortezza data, 2022);
- the main access portal, located near the Mules hamlet in the village of Campo di Trens, the site of various facilities and buildings for a total population of 2719 inhabitants (ISTAT, Campo di Trens data, 2022).

Detailed studies were performed in the period 2016–2020 concentrating on the Mules access tunnel. They included:
- a kriging estimation of rock and air tunnel temperature (Kasmaee et al., 2016);
- a feasibility study for installation of geothermal pipes between the first and secondary lining (Lanconelli, 2016; Lanconelli et al., 2018);
- an energetic, environmental, and economic assessment of alternatives for the efficient energy use of the exploited power, namely the supply of heat to nearby villages and the de-icing and snow melting of pavement at the Mules portal (Tinti et al., 2017).

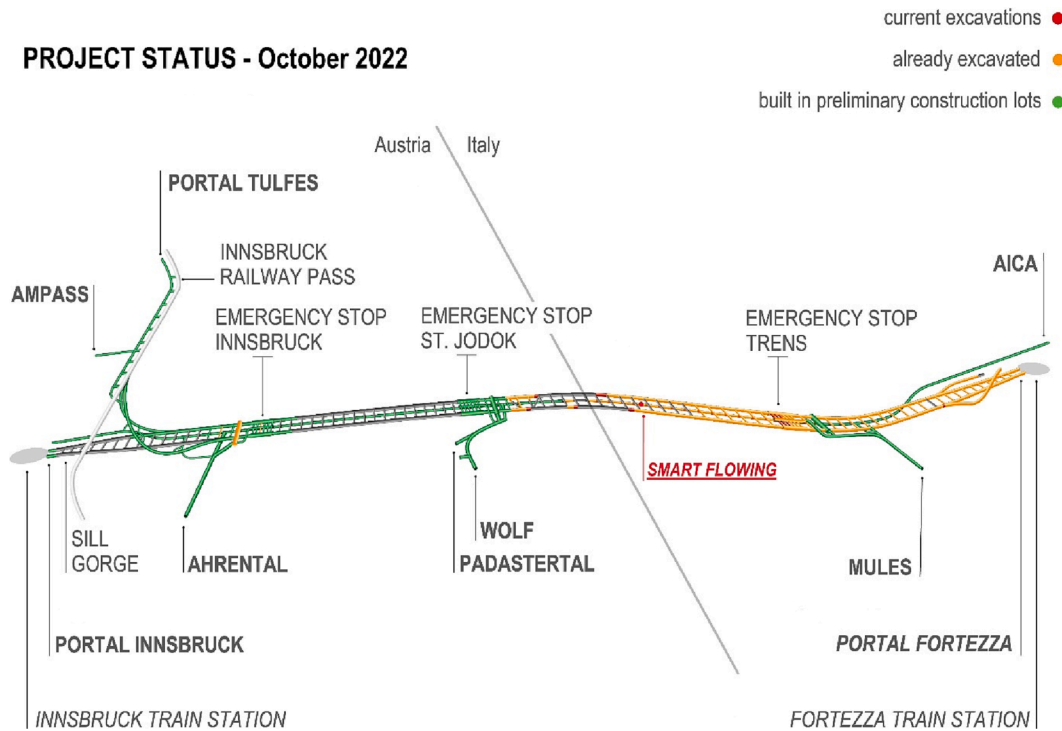More recently, increased attention has been devoted to the issue on

Fig. 1. Scheme of the BBT system, status of completion in October 2022 and location of the Smart Flowing prototype (modified from bbt-se.com).

the Austrian side of the BBT system. The research included estimations of the various discharges of drained water at the three portals of Wolf, Sillschlucht and Tulfes (Burger et al., 2022; Geisler et al., 2022).

The latest experimentation, conducted on the Italian side between 2020 and 2021, led to the design and implementation of the Smart Flowing prototype. The system was devised to thermally exploit the warm drainage water in an effective and sustainable way (Spaggiari, 2021; Spaggiari et al., 2022).

2. Materials and methods

2.1. Design parameters of the prototype

2.1.1. Smart Flowing layout

The prototype was placed inside the water drainage channel of the exploratory tunnel, formed by the two invert elements of the segmental lining. Specifically, the geothermal system is in contact with the invert lower segment, submerged by the drainage water flow and protected by the invert upper segment (Fig. 2).

Smart Flowing is envisioned as a new type of geothermal heat exchanger, belonging to the closed-loop system family of horizontal collectors (Fig. 3). The prototype has an overall length of 10.5 m and a total geothermal pipe length of about 76 m. It is composed by seven modules, which, linked together in series, create a single closed-loop collector. Each module is 1.5 m per 2 m and consists in a PE-Xa absorber pipe (outside diameter 25 mm and thickness 2.3 mm) arranged in a coil configuration and fixed over a rigid horizontal support made of a weldmesh and four steel profiles. The modules are connected through hydraulic and mechanical joints to form a continuous circuit in which the heat-carrier fluid flows.

To ensure the full immersion of the prototype in the drainage water, a steel dam was installed downstream to the system. The dam, in addition, was also effective in retaining silt material transported by the water, which created a protective cover of deposited material.

2.1.2. Initial measurements of drainage water flow temperature

Seven inspection pits allowed water temperature measurements at

any time along the length of Smart Flowing. Drainage water, deposited silt material over the pipe and even the pipe itself were reachable from a portable multi-parameter sensors device through the pits (Fig. 4). Measurements were then performed before, during and after all tests, to assess the natural state and variation induced by Smart Flowing. With regards to the initial natural state, the measurements provided a quite stable interval of values, ranging from 31.3 to 31.7 °C.

2.1.3. Preliminary calculation for selecting the testing and monitoring system

In order to put Smart Flowing into operation, specific testing and monitoring tools were connected to the circuit. Firstly, the continuous circulation of the heat transfer fluid (i.e. water) inside the absorber pipe had to be guaranteed. Secondly, the prototype's operation had to be tested and monitored in both heating and cooling modes.

The selected instrumentation consisted in a monobloc reversible air source heat pump (ASHP) unit, an auxiliary circulation pump and a storage tank. The initial design focused on the calculation of the hydraulic head for the water circulation pump, the exchangeable power for the reversible HP, and the volume for the water tank.

The pipe's total length, including the Smart Flowing system itself (about 75 m) and the return circuit outside the tunnel invert element, was calculated as 100 m. With a pipe's water content of 0.327 l/m (REHAU, 2013), the minimum volume of water tank was sized with a capacity of about 40 l.

Regarding the hydraulic head of the circulation pump, the contribution of the geodetic difference was neglected (the exploratory tunnel's slope is approximately 0.391 %), and the total head loss was calculated by considering both the concentrated (elbows, 180° return bends, unions and tees connection) and distributed head losses. The distributed head losses ΔH_d are obtained from the Hazen-Williams equation, which reads

$$\Delta H_d = 10.67 \frac{q^{1.85}}{C^{1.85} d^{4.87}} L \tag{1}$$

where q is the volumetric discharge in m³/s, d is the pipe diameter in m,
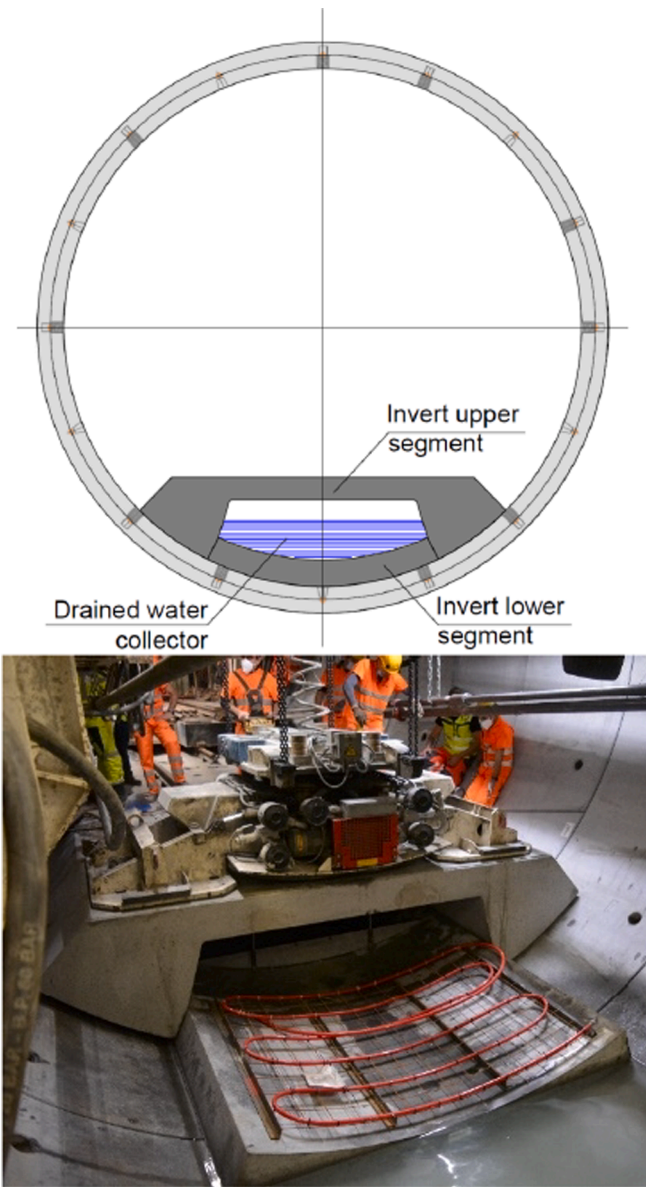
Fig. 2. Section of the exploratory tunnel and prototype location (left, modified from Spaggiari et al., 2022) and picture taken during the installation (right).

Fig. 3. Scheme of the Smart Flowing prototype (modified from Spaggiari et al., 2022).

L is the pipe length in m and C is the friction factor, accounting for the diameter and material of the pipe. According to Chase and Walsky (2003), for the investigated pipe, a value of C equal to 140 was used in Eq. (1). Volumetric water flow values from 1000 to 1500 l/h were considered, guaranteeing a purely turbulent flow. The formula accounting for concentrated head losses ΔH_c is written as

$$\Delta H_c = k \frac{v^2}{2g} \tag{2}$$

where k is the loss coefficient that depends on the pipe component, v is the velocity of the fluid, and g is the standard acceleration due to gravity. The loss coefficients assumed in the calculation are presented in Table 1.

These two factors gave the minimum total head of the hydraulic pump. For the hypothesized range of water flow, the head fell in a range from 6 m (1000 l/h) to 12 m (1500 l/h).

The dynamic calculation to obtain the capacity exchanged by the heat pump is described as follows. The thermal power variations were calculated step-by-step in a discrete way for each pipe segment i, and the total ther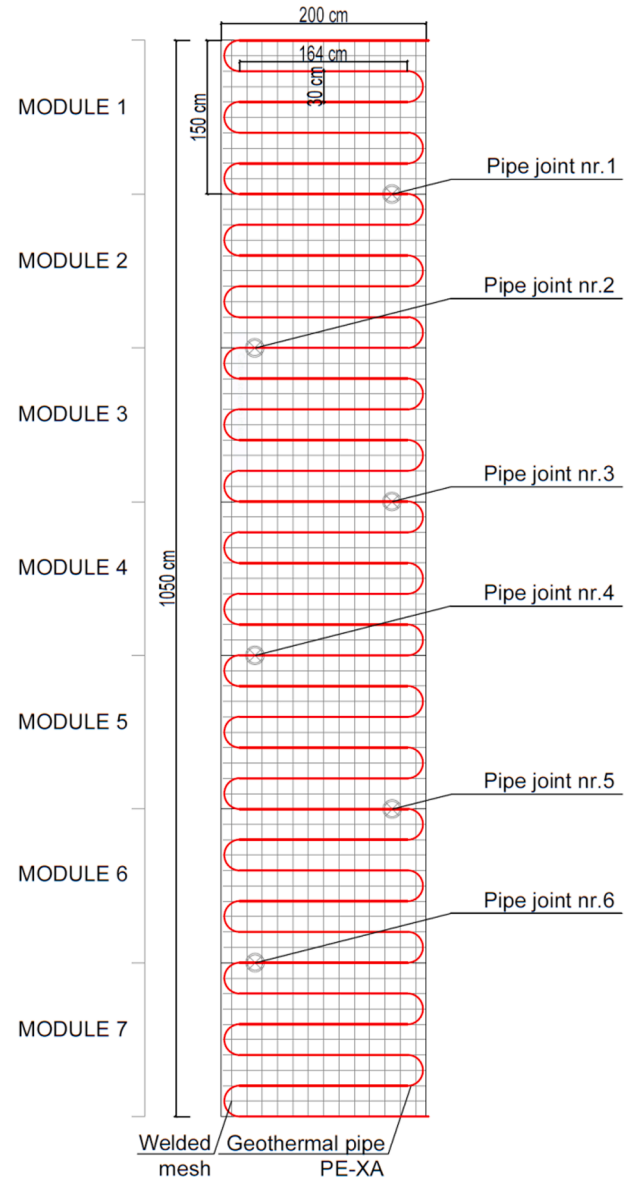mal power was obtained by cumulating the single segment contributions. The circuit was divided into fixed straight segments of 1-metre length for the 75 m of Smart Flowing. In this preliminary design, no thermal interferences along the meander path were assumed.

The equation to calculate the exchanged thermal power P_i at each segment in case of thermal conduction reads

$$P_i = \frac{T_{dw} - T_{f,i}}{R_{tot}} \tag{3}$$

where R_{tot} is the total thermal resistance, T_{dw} is the drainage water temperature, and $T_{f,i}$ is the fluid inlet temperature.

For the sake of simplicity, the power per meter exchanged by the circulating fluid in the absorber pipe was equally divided between the bottom part, facing the invert lower segment, and the top part, facing the invert upper segment (see Tinti et al., 2017; Lanconelli et al., 2018 for further details). The resulting equation is

$$P_i = \frac{1}{2} \cdot \frac{(T_{dw} - T_{f,i})}{R_{tot,b}} + \frac{1}{2} \cdot \frac{(T_{dw} - T_{f,i})}{R_{tot,t}} \tag{4}$$
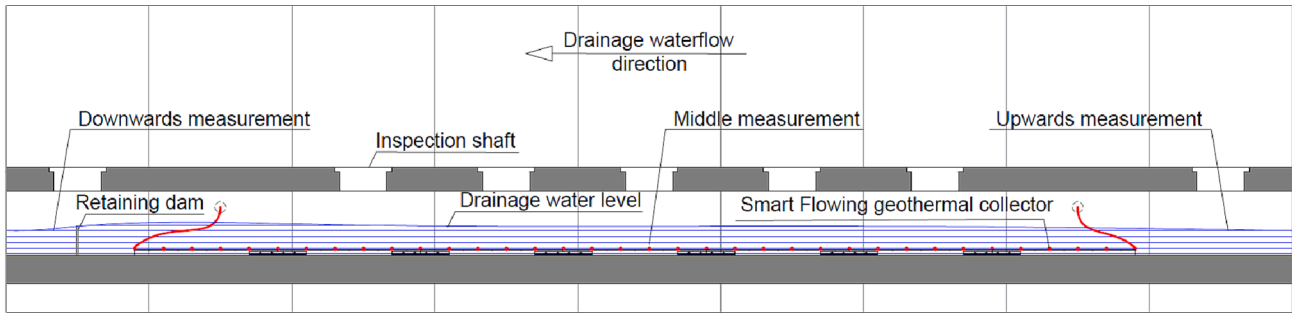
Fig. 4. Scheme of the location of the drainage water measurements (modified from Spaggiari et al., 2022).

Table 1
Concentrated head loss coefficients (Chase and Walsky, 2003).

Component	k (-)
Elbows - Regular 90°, flanged	0.30
Elbows - Long radius 90°, flanged	0.20
180° return bends, flanged	0.20
Tees - line flow, flanged	0.20
Union, threaded	0.08

where $R_{tot,b}$ and $R_{tot,t}$ are the "bottom" and "top" thermal resistances, respectively.

The expression to calculate the output fluid temperature $T_{f,o}$ at each segment is

$$T_{f,o} = T_{f,i} + \frac{P_i}{c_w q} \tag{5}$$

where q and c_w are respectively the flow rate and heat capacity of the water. It is worth noting that the outlet temperature of segment i is the inlet temperature of segment $i + 1$.

The total thermal resistance R_{tot} was calculated using the expression

$$R_{tot} = 2 \cdot \frac{1}{\frac{1}{R_{tot,b}} + \frac{1}{R_{tot,t}}} \tag{6}$$

which considers the absorber pipes as surrounded by a cylinder of saturated silt (the fine deposited material over Smart Flowing) with different thicknesses on the top (t) and bottom (b) sides. The total upper and lower resistances were obtained from

$$\begin{cases} R_{tot,b} = R_p + R_{g,b} \\ R_{tot,t} = R_p + R_{g,t} \end{cases} \tag{7}$$

where R_p is the pipe thermal resistance, $R_{g,b}$ is the "ground" thermal resistance at the bottom and $R_{g,t}$ is the "ground" thermal resistance at the top. The resultant upper and lower thermal resistance of each silt layer were calculated using Eq. (8) from Fourier's law

$$\begin{cases} R_{g,b} = \dfrac{\ln \dfrac{r_{out,b}}{r_{in,b}}}{2\pi\lambda} \\ \\ R_{g,t} = \dfrac{\ln \dfrac{r_{out,t}}{r_{in,t}}}{2\pi\lambda} \end{cases} \tag{8}$$

where r_{out} and r_{in} are the external and internal radius of the silt cover, calculated for both bottom and top layers. Due to the presence of groundwater, the thermal conductivity of the deposited material was considered as $\lambda = 3.0$ W/(mK), while the upper and lower thicknesses were measured as 20 and 5 cm, respectively. As such, the resulting thermal resistances were $R_{g,b} = 0.085$ (m·K)/W and $R_{g,t} = 0.150$ (m·K)/W. According to the construction details, the pipe's thermal resistance

was calculated as $R_p = 0.092$ (m·K)/W. Finally, the total thermal resistance of Smart Flowing resulted in $R_{tot} = 0.205$ (m·K)/W.

Once the boundary conditions and the thermal resistance were defined, it was possible to calculate the cumulative heating and cooling power and the associated final outlet temperatures. A drainage water temperature of 31.5 °C was assigned, in consideration of the measurements taken through the inspection shafts, at different times, while the water flow range in the pipe was kept from 1000 to 1500 l/h, in order to be coherent with hydraulic head calculation. The results are reported in Table 2.

It was assumed that, for a standard circulating flow comprised between 1000 and 1500 l/h and inlet temperature ranging from 10 to 50 °C, the expected thermal power was expected to be around −6.0 kW for extraction and 7.0 kW for injection.

It followed that the installation of an air source heat pump with maximum extraction and injection capacity of around 7 kW was advisable for testing Smart Flowing.

2.1.4. Design formula for the Smart Flowing prototype

As previously stated, the Smart Flowing prototype represents a unique installation designed for the BBT system: the meandering circuit is positioned in the space dedicated to the water drainage collection, thus exchanging heat with the surrounding silt deposit and water flow. Although the shape can resemble a classical horizontal geothermal heat exchanger (GHE), a generalized applicable method for sizing Smart Flowing and for calculating its heat transfer had to be developed.

The Italian standard related to the design and sizing requirements of heat pump geothermal systems (UNI 11466:2012) provides a formula for closed-loop horizontal GHEs installed in trenches. Given the resemblance of Smart Flowing's outline to a horizontal GHE, the technical standard was used as a starting point for design and modelling. New correction factors had to be considered to account for the thermal interference of meandering configuration subjected to drainage water flow. Based on the UNI11466:2012, the resulting equation reads

Table 2
Results of power and outlet temperature for different temperature and flow – simplified heat transfer dynamic model.

Flow (l/h)	Inlet Temperature (°C)	Outlet temperature (°C)	Power (kW)
1000	10	15.873	6.829
	50	44.947	−5.876
1100	10	15.412	6.922
	50	45.343	−5.956
1200	10	15.018	7.001
	50	45.682	−6.025
1300	10	14.677	7.069
	50	45.976	−6.083
1400	10	14.379	7.129
	50	46.232	−6.134
1500	10	14.117	7.180
	50	46.458	−6.178

$$P_{SF} = \frac{T_{dw} - \left(\frac{T_{f,i} + T_{f,o}}{2}\right)}{R'_{tot}} L_p \qquad (9)$$

where

- P_{SF} is the total thermal power output;
- L_p is the total length of the GHE;
- $T_{f,i}$ and $T_{f,o}$ are, respectively, the inlet and outlet temperatures of the heat carrier fluid;
- T_{dw} is the drainage water temperature;
- R'_{tot} is the modified total thermal resistance.

The thermal resistance in Eq. (9) is arranged to consider the specific features of Smart Flowing and of the specific heat exchange that takes place and was obtained as

$$R'_{tot} = \frac{2}{\frac{1}{R'_{tot,b}} + \frac{1}{R'_{tot,t}}} \qquad (10)$$

where the upper and lower resistance from Eq. (7) were updated to

$$\begin{cases} R'_{tot,b} = R_p + R_{g,b} \cdot F_l \cdot P_s \\ R'_{tot,t} = R_p + R_{g,t} \cdot F_l \cdot P_s \end{cases} \qquad (11)$$

The applied correction factors were F_l, accounting for the hours of HP operation per day, and P_s, expressing the influence of the pipe's diameter and the thermal interference resulting from the pipe's arrangement. F_l was also accounted for, since the thermal resistances of the layers around Smart Flowing are of impulsive type and are influenced by the impulse duration. P_s was obtained as a percentage variation of the pipe's diameter correction factor P_m, indicated in the technical standard UNI11466:2012, and considered as 0.990 as prescribed for similar horizontal GHEs. This value refers to a pipe layout similar to Smart Flowing, but buried in alluvial soil. Therefore, the parameter was modified to try to predict more accurately the thermal resistance and the expected exchanged power with the waterflow.

The modelling of the prototype required the determination of the corrective coefficient related to the dimensional and geometrical features of the absorber pipe. The calibrated correction factors are the result of a comparison between the power output obtained by the proposed analytical formula and the results from the 'dynamic' procedure presented in Section 2.1.2. The former implements Eq. (7), while the latter is obtained by Eqs. (3) and (4), considering the correction factors in the calculation of the total thermal resistance. The results given by the two formulae were compared with the data of an experimental water circulation test carried out on site and allowed to determine the calibrated parameters of the model: the load factor F_l result was 0.25 (i.e. six hours of daily operation) and the geometrical correction coefficient P_s was equal to 1.089 (i.e. a 10 % increment with respect to the value of P_m in the technical norm).

Table 3
Results of power and outlet temperature for different temperature and flow – calibration of parameters for the UNI11466 design method.

Flow (l/h)	Inlet Temperature (°C)	Outlet temperature (°C)	Power (kW)
1000	10	18.836	10.338
	50	42.397	−8.896
1100	10	18.828	10.341
	50	42.404	−8.898
1200	10	18.821	10.343
	50	42.410	−8.900
1300	10	18.815	10.345
	50	42.415	−8.901
1400	10	18.811	10.346
	50	42.419	−8.902
1500	10	18.806	10.347
	50	42.422	−8.904

The results presented in Table 3 are obtained by considering a saturated silt's thermal conductivity of 3.0 W/(m·K), a drainage water temperature of 31.5 °C, and an inlet temperature of 10 °C in extraction mode and 50 °C in injection mode in the dynamic analysis (assumed as the same values presented for the variables in Section 2.1.2). Results show that, considering the thermal interference of the meanders and the contribution of groundwater flow, the outlet temperature is 42.4 °C when injecting and 18.8 °C when extracting for 1000 l/h, providing a heat exchange of −8.9 kW and 10.3 kW, respectively.

2.2. Technical parts and installation

The layout design was governed both by space requirements and thermal considerations. In fact, the modules' dimensions are prescribed by the width and length of the invert segments. However, to achieve the highest possible heat exchange, Smart Flowing was designed in a coil configuration to maximise the temperature difference between the outlet and inlet pipe. When compared to other pipe arrangements, this configuration shows enhanced performances in presence of naturally high and stable temperatures, although thermal short-circuits could occur (Tinti et al., 2017; Lanconelli et al., 2018; Spaggiari et al., 2022).

The realization and installation of the Smart Flowing testing system was divided into the subsequent phases:

- the seven geothermal modules composing the Smart Flowing collector were assembled outside the exploratory tunnel and afterwards transported inside with the associated segments;
- the complete system was built up inside the exploratory tunnel concurrently to the placement of the invert segments;
- the heat pump, circulation pump and storage tank were installed on the tunnel lining intrados and connected to the Smart Flowing collector.

Considering the advanced construction stage of the exploratory tunnel, the geothermal system was designed to be easy to manufacture, to guarantee a functional set-up sequence in the TBM rail track placing area. The inverts were installed during the TBM advancement, a procedure remained unchanged during the Smart Flowing installation. On the other hand, the connection on-site between modules was realized through straight couplers, flat bars and bolts. Specifically, the procedure consisted in two operations: the fixing of the geothermal modules to the invert lower segment using wedge bolts and the connection of two subsequent geothermal modules using hydraulic fitting (push-fit PP straight coupler) for the piping and through flat bars and bolts for the L-profiles connection.

The installation sequence of Smart Flowing can be summarised in the following step-by-step procedure (Fig. 5):

1. placement of invert lower segment i;
2. installation and fixing of the geothermal module i over invert lower segment i;
3. placement of invert lower segment $i + 1$;
4. installation and fixing of the geothermal module $i + 1$ over invert lower segment $i + 1$ and connection between geothermal module i and geothermal module $i + 1$;
5. placement of invert upper segment i;
6. repetition of operations starting from point 3 with $i = i + 1$.

The installation inside the exploratory tunnel took place on the 4th and 5th of November 2020 and required two consecutive work shifts, due to an unrelated interruption of the TBM advancement on the first day. The entire installation procedure required 6 h and 40 min for an average of three workers, comprehensive of the standard handling of the segments. It is worth noting that most of these procedures were overlapping with those carried out for the standard TBM advancement. Finally, the time dedicated to the geothermal system setup was 2 h and
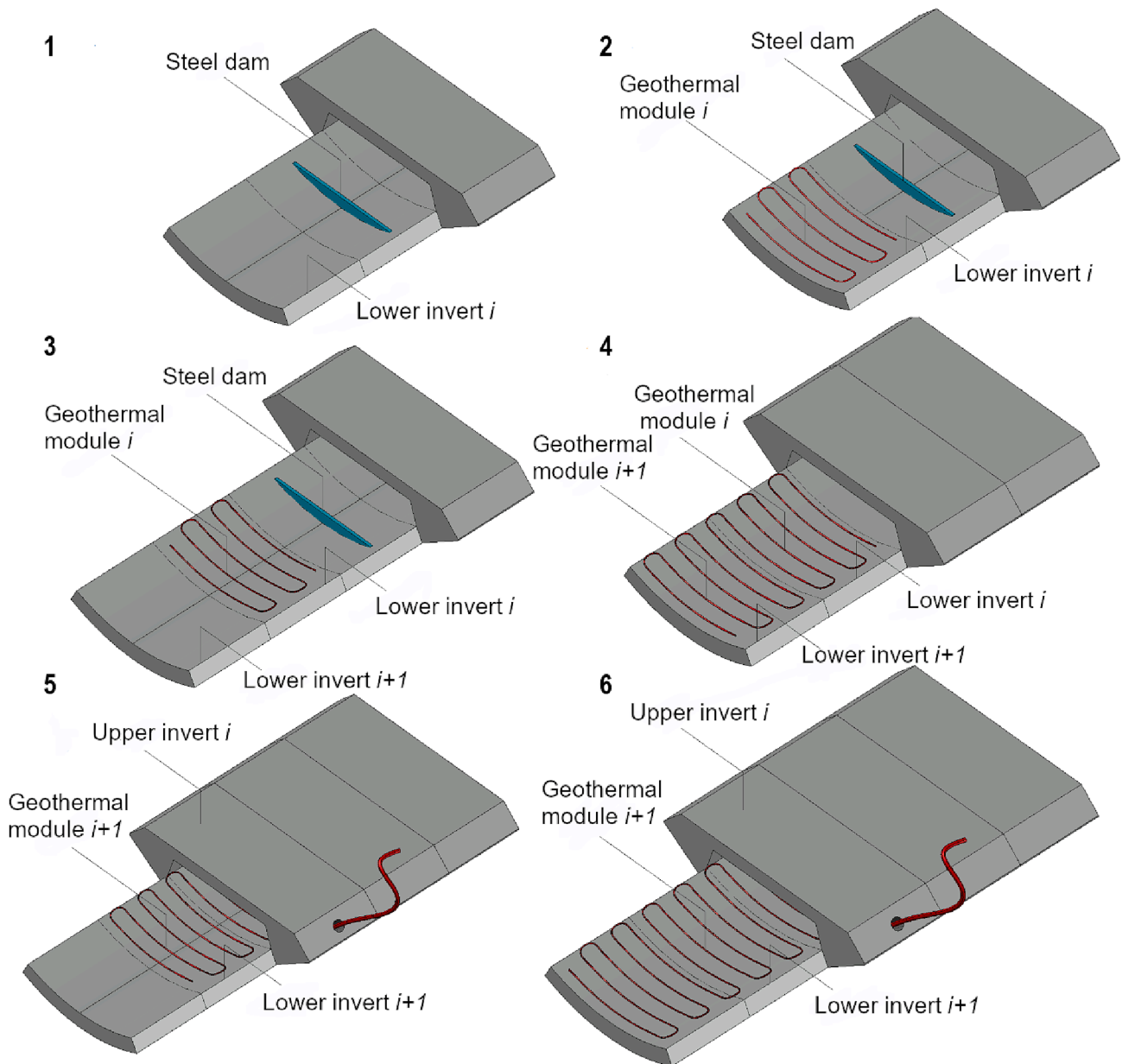
Fig. 5. Installation sequence of the Smart Flowing prototype (modified from Spaggiari et al., 2022).

20 min, about one third of the total installation time.

Both the installation of the geothermal circuit and the testing and monitoring system were subjected to strict operative rules and needed to comply with structural, logistical and safety requirements. As the modules of the heat exchanger were developed to avoid delays and hindrances to the advancement of the TBM, the positioning of the testing system was conceptualised to prevent obstruction during the transit of the shuttle trains or emergency operations.

The heat pump model NAW006, provided by ENEREN s.r.l., is a reversible water-to-air HP having a scroll brushless DC compressor, electronically controlled fans, an electronic expansion valve and an internal circulation low hydraulic head pump. It is a HP unit generally installed in buildings to produce cooling, heating and hot water. Additionally, sensors constantly record the heat-carrier fluid flow and its inlet and outlet temperatures, the ambient temperature, and the water temperature inside the water tank, as well as many other machine parameters (pressure, fan speed, compressor frequency, etc.).

The monobloc HP is 133 cm in length, 57 cm in depth and 118 cm in height (Fig. 6a). It has a capacity of 7.3 kW in injection mode and 6.0 kW

in extraction mode. The performance related to each capacity value is given in Table 4. The installed model has a lower capacity than that described in the preliminary calculations, which was a consequence of the reduced available space inside the exploratory tunnel. However, with such values, the system was expected to perform efficiently.

Monitoring instruments to measure the temperature and flow are integrated inside the heat pump device, thus further reducing the space required by the heat pump located inside the exploratory tunnel and facilitating the monitoring operations.

The additional external components installed for Smart Flowing to function are:

- an 80-litre inertial storage tank for hot/cold water, made of carbon steel with a high-density rigid polyurethane foam insulation, with external diameter of 46 cm and height of 86 cm, a maximum operating pressure of 5 bar and a maximum/minimum operating temperature of 90/-10 °C (Fig. 6b). It can also host water temperature monitoring sensors;
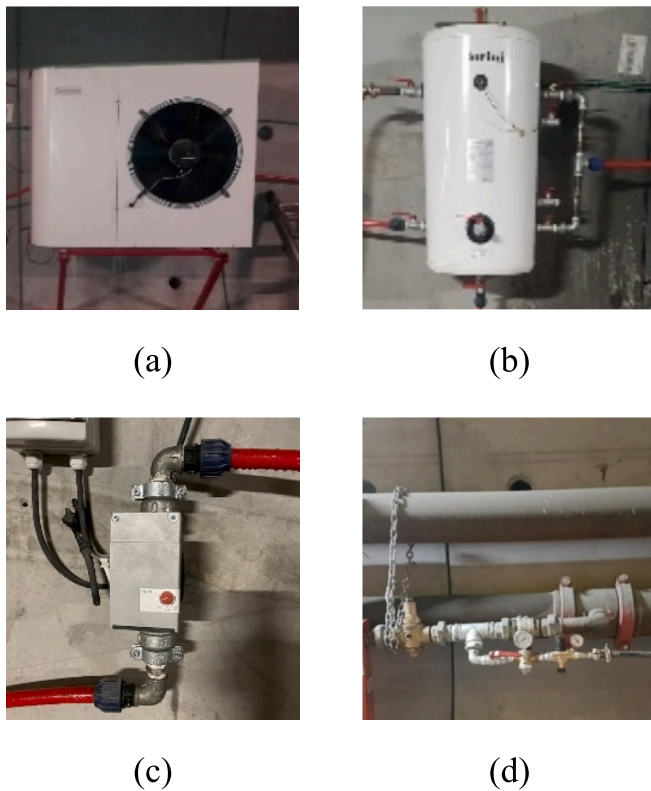
(a)

(b)

(c)

(d)

Fig. 6. Details of Smart Flowing testing system: heat pump (a); storage tank (b); circulation pump (c); automatic fill unit (d).

Table 4
ASHP technical data (EN14511-2) (ENEREN, 2021a).

Working mode	Capacity (kW)	COP/EER (-)
Heat injection mode	7.3	4.21
Heat extraction mode	6.0	3.69

- a wet rotor circulator with integrated differential pressure regulation and Electronic Commutated Motor (ECM), with 7.7 m maximum delivery head for a 25 mm pipe, a maximum volume flow of 8760 l/h and an overall machine length of 18 cm (Fig. 6c). It includes the option of transferring the pressure head to the water constantly or variably at different levels;
- an automatic fill unit, which connects the main hydraulic system of the exploratory tunnel with the tank, to prevent pressure losses in the circuit (Fig. 6d).

2.3. Tests performed

The activation of the air-to-water HP allows the assessment of the performance of the prototype in two different scenarios:

- in heat extraction mode, the cold water circulated inside the loop, heating up. It was used to evaluate the heat exploitation potential of Smart Flowing;
- in heat injection mode, the hot water circulated into the piping, cooling down. This stage was essential to quantify the heat dissipation potential of the system.

Moreover, additional manometers and thermometers were placed at the top of Smart Flowing. Throughout the tests, both the working mode and off-mode phases were monitored. In particular, the off-mode was used to quantify the heat release potential, obtained through circulation

of water inside Smart Flowing up to returning to the initial temperature.

The main variables governing all tests were the water return temperature to the HP (i.e. the T_{in} HP limit), manually fixed as set-point and measured at the HP inlet pipe, and the hydraulic head of the external water circulation pump. T_{in} HP limit was set over a wide range of variations passing from 5 °C in heat extraction mode to 52 °C in heat injection mode. The auxiliary water circulation pump was always set on a constant pressure head mode, with variable values from 2 to 4 m.

Equation (12) is used to calculate the extracted/injected power

$$P_{SF,test} = c_p \cdot \rho \cdot q \cdot \Delta T \tag{12}$$

where $P_{SF,test}$ is the exchanged power, c_p and ρ are the heat capacity and density of the heat-carrier fluid, q is the circulating water flow and ΔT is the difference between the inlet and outlet temperatures. The related energy was obtained as the cumulation of the extracted power during the prototype working phase.

As the drainage water flow and temperature boundary conditions represent fundamental parameters to perform proper and successful comparisons among tests, at the beginning of the experimentation some tests were repeated to verify the repeatability of results in terms of circulating flow temperature due to heat injection/extraction and the stability of the testing and monitoring system. In particular, injection tests number 1 and 2 were repeated for a similar duration and were compared resulting in substantially similar behaviour.

Table 5 lists the tests performed during the two-month monitoring period. The eleven tests are characterised by several set-point temperatures, variable duration and adjustable hydraulic pump head.

3. Results

3.1. Results of the test campaign

The results of the tests are summarised from Table 6 to 16. The tables provide information about the HP working stage, the recorded temperature at the inlet and outlet of the HP and working fluid flow, and the calculated exchanged power as well as the cumulated energy for each test.

Test 1 and 1bis had a set-point temperature of 52 °C resulting in extremely similar temperature trends and stabilisation temperatures. However, in test 1 the recovery state was not recorded. Also, test 8 and 8bis were performed at an inlet HP set-point of 52 °C with a different time frame, so as to capture the recovery phase and verify the stability of the temperature limit for a prolonged duration. Both tests resulted in a comparable temperature stabilisation. Although the injection tests at a T_{in} HP limit of 40 °C (test 2 and 2bis) had a different duration, the temperature results overlapped in all the phases, as expected. Tests from 3 to 5 resulted in a stabilisation temperature of about 13.5 °C, never reaching the set-point at 10 °C. Irrespective of the duration, the extraction tests were characterised by similar trends. Furthermore, Tables 13 and 14 summarise the results of long-term extraction tests, i.e.

Table 5
List of performed test and main results.

Test No.	Duration	Heat mode	Circulation pump head (m)	T_{in} HP limit (°C)
1	2 h30	Injection	4	52
1bis	3 h30			
2	3 h20	Injection	4	40
2bis	4 h			
3	3 h	Extraction	4	10
4	24 h	Extraction	4	10
5	70 h	Extraction	2	10
6	74 h	Extraction	2	5
7	100 h	Extraction	2	5
8	16 h	Injection	2	52
8bis	2 h40			

Table 6
Results of heat injection test n°1 with set-point temperature at 52 °C and 2 h and a half duration with no recorded recovery state.

Injection test 1 - T_{in} HP limit 52 °C						
Time (h)	Working state	T_{in} HP (°C)	T_{out} HP (°C)	Power (kW)	Flow (l/h)	Cumulated energy (kWh)
0.43	On	28.80	32.10	−5.11	1332.00	−0.02
0.59	On	34.20	39.70	−8.71	1362.00	−1.30
0.79	On	39.80	45.00	−8.42	1392.00	−3.01
1.36	On	48.00	53.00	−8.34	1434.00	−7.72
1.50	On	48.70	53.20	−7.41	1416.00	−8.77
2.30	On	49.30	53.40	−6.69	1404.00	−13.58

Table 7
Results of heat injection test n°1bis with set-point temperature at 52 °C and 3 h and a half duration, including 1-hour recovery state.

Injection test 1bis - T_{in} HP limit 52 °C						
Time (h)	Working state	T_{in} HP (°C)	T_{out} HP (°C)	Power (kW)	Flow (l/h)	Cumulated energy (kWh)
0.40	On	30.20	35.50	−8.21	1332.00	−0.35
0.55	On	35.80	41.60	−9.19	1362.00	−1.67
0.67	On	39.70	45.20	−8.71	1362.00	−2.71
1.03	On	46.40	52.10	−8.83	1332.00	−5.95
2.23	On	49.60	53.80	−6.80	1392.00	−14.60
3.30	Off	35.80	35.80	−	1278.00	−

Table 8
Results of heat injection test n°2 with set-point temperature at 40 °C and 3 h and 20 min duration, including 1.5 h recovery state.

Injection test 2 - T_{in} HP limit 40 °C						
Time (h)	Working state	T_{in} HP (°C)	T_{out} HP (°C)	Power (kW)	Flow (l/h)	Cumulated energy (kWh)
0.40	On	29.90	35.40	−8.52	1332.00	−0.37
0.50	On	34.30	40.00	−8.83	1332.00	−1.25
1.00	On	39.50	41.90	−3.52	1260.00	−3.87
1.67	On	39.20	42.00	−2.80	1332.00	−5.93
1.77	On	39.60	41.90	−2.30	1302.00	−6.32
3.40	Off	31.90	31.90	−	1260.00	−

Table 9
Results of heat injection test n°2bis with set-point temperature at 40 °C and 4 h duration, including 1 h recovery state.

Injection test 2bis - T_{in} HP limit 40 °C						
Time (h)	Working state	T_{in} HP (°C)	T_{out} HP (°C)	Power (kW)	Flow (l/h)	Cumulated energy (kWh)
0.44	On	30.90	36.80	−9.06	1320.00	−0.58
0.89	On	39.60	42.50	−4.49	1332.00	−3.30
1.45	On	39.80	42.40	−4.03	1332.00	−5.05
2.41	On	39.60	41.90	−3.59	1344.00	−7.69
2.80	On	41.00	44.30	−5.23	1362.00	−9.28
4.00	Off	33.30	33.30	−	1320.00	−

Table 10
Results of heat extraction test n°3 with set-point temperature at 10 °C and 3 h duration, including 30 min recovery.

Extraction test 3 - T_{in} HP limit 10 °C						
Time (h)	Working state	T_{in} HP (°C)	T_{out} HP (°C)	Power (kW)	Flow (l/h)	Cumulated energy (kWh)
0.37	On	29.10	25.00	6.21	1302.00	0.18
0.50	On	25.60	20.00	8.40	1290.00	1.25
0.73	On	20.00	15.00	7.43	1278.00	3.08
1.08	On	16.70	12.00	6.89	1260.00	5.56
1.70	On	14.50	10.00	6.59	1260.00	9.64
2.15	On	13.90	9.50	6.45	1260.00	12.58
3.00	Off	23.90	23.90	−	1278.00	−

74 h (test 6) and 100-hour (test 7) for a set-point return temperature of 5 °C. Test 6 and 7 are comparable in the temperature decreasing and stabilisation phases, while 6 h of recovery phase were recorded only for test 7.

For the tests from 5 to 8bis the hydraulic head for the circulation pump was reduced from 4 to 2 m. It did not significantly affect the total exchanged power, neither for injection nor for extraction tests.

All the tests showed that the set-point temperature was attained only for isolated peaks and the stabilisation temperature reached a plateau at values higher/lower than the limit after a long time. The results could be explained by the continuous flow of the drainage water: its heating and cooling dissipation potential proves the sustainability of Smart Flowing at the given working temperatures. For instance, the inlet temperature did not reach the 5 °C set point limit even after 45 operating hours (test 7), while the inflow working fluid peaked to 52 °C after 10 h, followed by a light decrease (test 8).

Table 11
Results of heat extraction test n°4 with set-point temperature at 10 °C and 24 h duration with no recorded recovery.

Extraction test 4 - T_{in} HP limit 10 °C						
Time (h)	Working state	T_{in} HP (°C)	T_{out} HP (°C)	Power (kW)	Flow (l/h)	Cumulated energy (kWh)
0.20	On	25.80	20.20	8.32	1278.00	1.10
1.20	On	15.40	10.90	6.59	1260.00	8.23
5.00	On	13.70	9.50	6.09	1248.00	32.43
10.00	On	13.60	9.50	6.01	1260.00	63.23
15.00	On	13.50	9.40	5.95	1248.00	93.81
22.00	On	13.40	9.40	5.80	1248.00	134.86
24.00	On	13.30	9.40	5.71	1260.00	146.25

Table 12
Results of heat extraction test n°5 with set-point temperature at 10 °C and 70 h duration with no completely recorded recovery.

Extraction test 5 - T_{in} HP limit 10 °C						
Time (h)	Working state	T_{in} HP (°C)	T_{out} HP (°C)	Power (kW)	Flow (l/h)	Cumulated energy (kWh)
0.15	On	26.00	20.10	8.27	1206.00	0.85
2.25	On	14.30	9.60	6.43	1176.00	12.65
10.00	On	13.80	9.30	6.15	1176.00	60.63
20.00	On	13.70	9.20	6.15	1176.00	121.08
50.00	On	13.40	9.30	5.61	1176.00	292.25
68.00	On	13.60	9.30	5.79	1158.00	395.55
70.00	Off	16.50	16.30	–	1176.00	–

Table 13
Results of heat extraction test n°6 with set-point temperature at 5 °C and 74 h duration with no completely recorded recovery.

Extraction test 6 - T_{in} HP limit 5 °C						
Time (h)	Working state	T_{in} HP (°C)	T_{out} HP (°C)	Power (kW)	Flow (l/h)	Cumulated energy (kWh)
0.22	On	25.80	19.50	8.31	1116.00	1.13
2.25	On	14.20	9.20	6.24	1074.00	14.76
10.00	On	10.00	8.20	5.99	1074.00	62.09
20.00	On	13.20	8.30	6.12	1074.00	123.21
50.00	On	12.70	8.00	6.10	1116.00	302.14
68.00	On	12.80	8.10	6.03	1104.00	410.03
74.00	Off	16.20	16.00	–	1116.00	–

Table 14
Results of heat extraction test n°7 with set-point temperature at 5 °C and 100 h duration, of which about 6 h recovery.

| Extraction test 7 - T_{in} HP limit 5 °C						
Time (h)	Working state	T_{in} HP (°C)	T_{out} HP (°C)	Power (kW)	Flow (l/h)	Cumulated energy(kWh)
0.04	On	25.60	24.60	1.32	1134.00	0.01
0.07	On	25.60	20.70	6.46	1134.00	0.16
0.27	On	20.60	15.00	7.27	1116.00	1.66
0.55	On	17.10	12.00	6.72	1134.00	3.62
0.94	On	14.80	10.00	6.23	1116.00	6.11
2.44	On	13.30	8.50	6.23	1116.00	15.37
44.46	On	12.30	7.70	5.91	1104.00	269.19
70.00	On	12.70	8.00	6.03	1104.00	421.67
93.80	On	12.70	8.20	5.78	1104.00	564.25
100.00	Off	29.10	29.10	–	1146.00	–

Table 15
Results of heat injection test n°8 with set-point temperature at 52 °C and 16 h duration with no recorded recovery state.

| Injection test 8 - T_{in} HP limit 52 °C						
Time (h)	Working state	T_{in} HP (°C)	T_{out} HP (°C)	Power (kW)	Flow (l/h)	Cumulated energy (kWh)
0.07	On	29.70	35.40	−7.60	1146.00	−0.21
0.19	On	33.90	40.30	−8.75	1176.00	−1.30
0.37	On	39.00	45.00	−8.29	1188.00	−2.82
0.84	On	45.90	52.00	−8.43	1188.00	−6.79
5.00	On	49.40	54.30	−6.77	1188.00	−36.60
6.00	On	49.60	54.60	−7.01	1206.00	−43.49
10.22	On	51.90	57.40	−7.60	1188.00	−72.80
11.24	On	52.00	57.70	−7.87	1188.00	−79.54
16.00	On	49.40	54.60	−7.11	1176.00	−110.23

Table 16
Results of heat injection test n°8bis with set-point temperature at 52 °C and 2 h and 40 min duration with partially recorded recovery state.

Injection test 8bis - T_{in} HP limit 52 °C						
Time (h)	Working state	T_{in} HP (°C)	T_{out} HP (°C)	Power (kW)	Flow (l/h)	Cumulated energy (kWh)
0.22	On	35.10	42.10	−9.33	1146.00	−1.50
0.60	On	44.20	50.70	−8.75	1158.00	−4.94
1.00	On	48.50	54.50	−8.08	1158.00	−8.39
1.63	On	49.20	53.70	−6.06	1158.00	−13.04
2.60	Off	35.50	35.50	–	1146.00	–
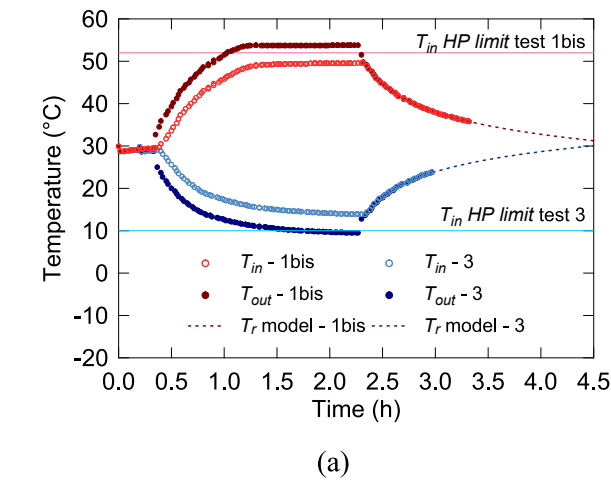
(a)
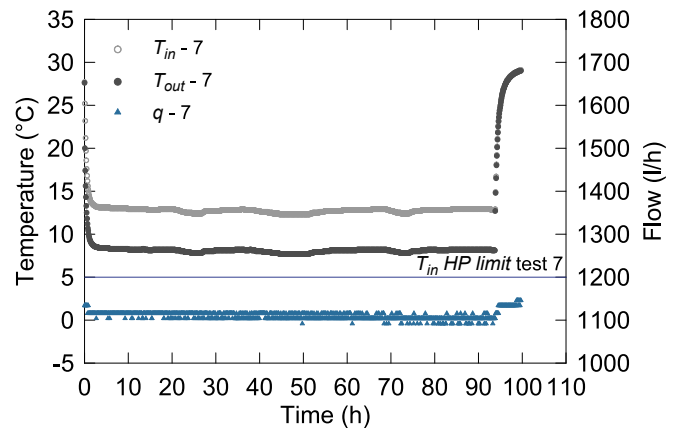
(b)

Fig. 7. Temperature and flow (a), and energy and power (b) evolution during tests 1bis and 3.

(a)

(b)

Fig. 8. Temperature and flow (a), and energy and power (b) evolution during tests 7.

Fig. 7 shows the measurements and calculation from test 1bis and test 3. Fig. 7a shows the inlet and outlet temperature, together with circulating water flow, while Fig. 7b presents the calculated energy and power. The general trend of both tests is divided in an increasing/decreasing temperature phase, followed by stabilisation of the temperatures and then fast temperature recovery (T_r) whenever HP switched off.

Fig. 8 presents the long-term behaviour recorded during test 7. Fig. 8a presents inlet and outlet temperature and flow, while, similarly to Fig. 7b, Fig. 8b shows energy and power.

Table 17, as a resume of the whole testing campaign, summarises the following variables: maximum power, cumulated energy, average power and temperature of stabilisation.

During the stabilisation phase, the resulting average powers were mainly limited by the capacity of the HP and the difference in temperature between the set-point and the drainage water. For a T_{in} HP limit of

52 °C, the average injected power reached almost the limit capacity of the HP (i.e. 7.3 kW) in tests 1 and 1bis, and, later, in tests 8 and 8bis. The temperature stabilisation was slightly lower (around 49 °C), suggesting a possible slight increase in capacity, with respect to the capacity of the HP. Repeating the injection tests with a lower T_{in} HP limit of 40 °C (tests 2 and 2bis), the temperature difference between the set-point and the drainage water sank to 10 °C, and this resulted in about half the exchanged power with respect to the previous mentioned tests. In this case, the power stabilisation was given by the temperature constraints of the machine. In all extraction tests conducted (tests from 3 to 7) it was observed that, no matter the set-point variations from 10 to 5 °C, the temperature limit was never reached, and the average extracted power was always around 6.0 kW, the limit capacity of the machine. This proves that the heat exploitation potential of Smart Flowing is higher than the maximum request during the tests.

These general conclusions can be drawn from the performed tests:

Table 17

Main results of performed tests.

Test No.	Max. Power (kW)	Cumulated Energy (kWh)	Aver. Power (kW)	T_{in} HP stabilisation (°C)
1	−8.71	−13.58	−6.90	49.30
1bis	−9.19	−14.94	−6.50	49.50
2	−9.14	−6.32	−3.80	39.60
2bis	−9.60	−9.28	−3.60	39.70
3	8.48	13.47	6.50	14.00
4	8.32	146.25	6.00	13.60
5	8.27	408.21	5.90	13.60
6	8.31	444.60	6.00	12.90
7	7.65	564.25	6.00	12.70
8	−8.89	−110.23	−7.00	49.50
8bis	−9.33	−13.04	−7.50	49.00

- the system performed better in extraction mode rather than in injection mode, since the time intervals needed to reach a selected HP temperature limit were shorter in injection with respect to extraction;
- the relatively high temperature of the drainage water (i.e. 31–32 °C) significantly favoured the extraction mode;
- during the stabilisation phase, the average exchanged power was governed by both the HP capacity and the fluid temperature limits in injection mode, while in extraction tests the power solely depended on the HP capacity, suggesting that additional heat could be exploited;
- the recovery phase happens to be governed by the drainage water – being the indirect source of geothermal energy – which continuously flows and enables the heat carrier fluid to return to its natural state temperature in 2–3 h;
- the choice of different hydraulic head of the external water circulation pump did not significantly influence the total exchanged power.

3.2. Modelling based on test results

Once the design Eq. (9) for the Smart Flowing collector was defined, it was possible to verify its accuracy based on the results of the performed tests (Section 3.1). Starting from Eq. (13), the experimental thermal resistance R_{test} was calculated from the measurements of the recorded tests during the stabilisation phase as:

$$R_{test} = \frac{T_{dw} - \left(\frac{T_{f,i}+T_{f,o}}{2}\right)}{P_{SF,test}} \cdot L_p \qquad (13)$$

where T_{dw} is the drainage water temperature, $T_{f,i}$ and $T_{f,o}$ are the inlet and outlet heat carrier fluid temperature, L_p is the prototype's length and $P_{SF,test}$ is the total exchanged thermal power over a limited stabilisation interval. Specifically, the drained water temperature was measured at about 31.5 °C and the inlet and outlet temperatures and power output of the HP were used as the mean values obtained from the stabilisation phase. The thermal resistance R_{test} is then compared with the theoretical thermal resistance R'_{tot} of Eq. (10). The calculations of the reference resistance R'_{tot} were realized for all the conducted tests. The parameter F_l, accounting for the operating hours of the HP per day, was imposed equal to 1, since the performed tests were conducted without interruptions. The length of the pipe L_p and the parameter P_s (expressing the mutual influence of pipes' thermal resistance in the circuit, i.e. 1.287) were kept equal to those of the original design (Section 2.1.3).

Results of the experimental thermal resistance R_{test} for the various tests performed are presented in Table 18 in comparison with the theoretical initial thermal resistance R'_{tot} (i.e. 0.237 m·K/W). Inspection of the table reveals that the experimental total thermal resistance R_{test} showed a wide variation, with different values for each test, and was generally different from the design thermal resistance R'_{tot} from 5 to 30 % in absolute numbers.

The difference with respect to design values, due to the varying convective conditions of the drainage water, led to the introduction of an iterative approach to better define the design parameters of the system. Consequently, modelling of Smart Flowing was modified based on the test results. Specifically, the difference between the water flow temperature (T_{dw}) and the heat-carrier fluid temperature set as a limit of the HP (i.e. set-point temperature, $T_{in\ HP,\ limit}$) was used as new indicator

Table 18

Calculation of the experimental thermal resistance R_{test} and comparison with R'_{tot}.

Test No.	T_{in} HP limit (°C)	$T_{f,i}$ (°C)	$T_{f,o}$ (°C)	P_{test} (kW)	R_{test} (mK/W)	Difference (%)
1	52.00	49.18	53.37	−6874.81	0.265	12.01
1bis	52.00	49.46	53.55	−6481.34	0.285	20.16
2	40.00	39.45	41.99	−3821.52	0.229	−3.42
2bis	40.00	39.68	41.90	−3562.00	0.247	4.39
3	10.00	14.01	9.68	6510.31	0.265	11.75
4	10.00	13.55	9.43	6010.37	0.292	23.28
5	10.00	13.61	9.27	5892.69	0.299	26.05
6	5.00	12.88	8.14	6057.99	0.304	28.45
7	5.00	12.72	8.06	6003.07	0.309	30.40
8	52.00	49.51	54.52	−6928.54	0.273	15.18
8bis	52.00	49.04	54.47	−7333.36	0.255	7.49

Table 19

Calculation of the corrected parameter P_s.

Set-point temperature (°C)	$|T_{in}$ HP limit - $T_{dw}|$ / T_{dw} °C (%)	Corrected parameter P_s [-]
52.00	65.08	1.634
40.00	26.98	1.257
10.00	68.25	1.666
5.00	84.13	1.823

Table 20
Comparison of the experimental thermal resistance R_{test} with the resistance calculated using P_s.

Test No.	P_s (-)	$R_{tot,mod}$ (mK/W)	R_{test} (mK/W)	Difference (%)
1	1.634	0.275	0.265	−3.54
1bis	1.634	0.275	0.285	3.48
2	1.257	0.234	0.229	−2.06
2bis	1.257	0.234	0.247	5.86
3	1.666	0.279	0.265	−4.96
4	1.666	0.279	0.292	4.85
5	1.666	0.279	0.299	7.21
6	1.823	0.296	0.304	2.88
7	1.823	0.296	0.309	4.44
8	1.634	0.275	0.273	−0.81
8bis	1.634	0.275	0.255	−7.43

to define the thermal resistance. Since the drained water flow during the tests was constant, the original design value of the parameter P_s was scaled based on this. Eq. (14) to calculate P_s reads

$$P_s = P_m \cdot \left(1 + \frac{|T_{inHP,limit} - T_{dw}|}{T_{dw}}\right) \tag{14}$$

where P_m is the corrective coefficient accounting for the pipe diameter, $T_{in\ HP,\ limit}$ is the set-point temperature and T_{dw} is the temperature of the drainage water.

According to the tests, four different temperature scenarios were experimentally reproduced (52, 40, 10, 5 °C). Therefore, four possible values of the corrective parameter P_s were obtained, as explained in Table 19.

By applying the updated values of P_s to the calculation of convective thermal resistance of Equation (14), new values of R'_{tot} were found ($R'_{tot, mod}$). The corresponding difference between calculated and experimental thermal resistance was (in absolute terms) in the 1–8 % range, with a mean variation of 4.3 % (Table 20).

The design parameters are obtained starting from the experimental results given by the performed tests. Therefore, the generalization of Smart Flowing heat exchange design criteria needs further modelling. In order to fully understand the heat transfer mechanism due to
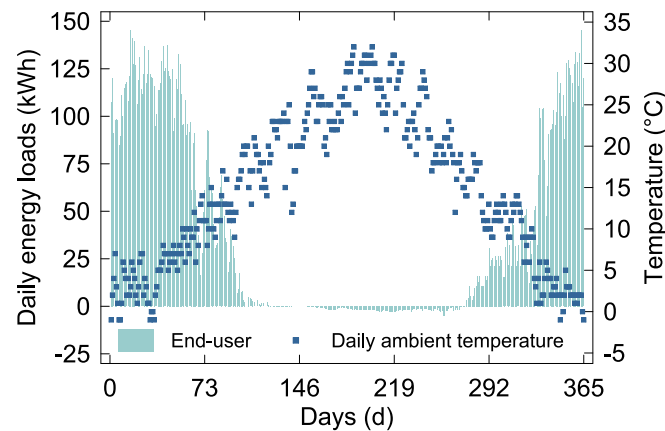

Fig. 9. Daily energy load of a fictitious end-user, with 10 kW of peak power, located in the climatic area of Brenner Base Tunnel.

Table 21
GSHP technical data (EN14511, condenser 30/35 °C) (ENEREN, 2021b).

Mode	Evaporator inlet/outlet temperature (°C)	Capacity (kW)	*COP/EER* (-)
Cooling	12/7	6.7	3.94
	23/18	9.9	6.03
Heating	0/-3	7.0	4.31
	10/5	8.9	5.63

convection, Computational Fluid Dynamics (CFD) modelling is planned. The drainage water flow and its interaction with Smart Flowing will be simulated in future works, in order to validate the hypotheses done in the present work.

3.3. Dynamic application of the prototype to a final user case study

Tests conducted with the experimental prototype have provided preliminary indications for further practical installation in real tunnel applications. The results have shown that the heat (and cool) dissipation potential of the drained water is huge, varying according to the water temperature level. For the specific case study, with drained water temperature above 31 °C and for long-term stabilized temperature above 13.5 °C (as in Fig. 8), the circulating fluid flow in the closed loop proved to be quite high compared to standard closed loop applications, both vertical and horizontal. In order to provide a preliminary estimation of Smart Flowing heating potential in the climatic conditions of the Brenner Base Tunnel, the climatic and end-user need data from Tinti et al. (2017) were used. Moreover, the current heating system (individual gas furnaces) of the BBT SE offices in Fortezza (BZ) was chosen as a benchmark for evaluation of the energy performance of Smart Flowing and comparison with fossil fuel alternatives (Spaggiari et al., 2022).

The daily energy needs of a hypothetical final user along the year were simulated, considering 10 kW of peak power as a realistic value and by assuming heat source peaks in the range of 6–8 kW for both injection and extraction modes, consistently with the results of the Smart Flowing experimental campaign. Fig. 9 shows the evolution of energy needs of the hypothetical consumer, together with average daily ambient temperature of the climatic zone of interest.

According to the calculations, the total heat requested by the end-user is 14,087 kWh/year, while the total energy for refrigeration is −205 kWh/year.

Starting from the energy load and using the Smart Flowing performed tests' results (Section 3.1), it was possible to:

- select a suitable option for a hypothetical Ground Source Heat Pump (GSHP), connected to the prototype, to provide heat to the final consumer;
- simulate the daily functioning of Smart Flowing for different kinds of distribution and emission systems, working at 35 °C, 45 °C and 55 °C.

The model of GSHP used for simulating the performance of Smart Flowing was the GSE006 from ENEREN s.r.l., of similar capacity to the ASHP used for testing. Table 21 describes the basic performances of the GSHP, with respect to working temperatures and capacity.

For each time step of the energy request, it was possible to get the expected extracted/injected energy from Smart Flowing according to the temperature/performance table (ENEREN, 2021b) through Eq. (15)

$$SF_{ext,j} = E_{heat,j} - \frac{E_{heat,j}}{COP_j} = E_{heat,j} - L_{heat,j}$$

$$SF_{inj,j} = E_{cool,j} - \frac{E_{cool,j}}{EER_j} = E_{cool,j} - L_{cool,j} \tag{15}$$

where, for each time step j, E is the requested energy from the end-user (heating E_{heat}, cooling E_{cool}); L is the electric energy absorbed by the heat pump (heating L_{heat}, cooling L_{cool}); SF is the energy exchanged between Smart Flowing and the drained water (extraction SF_{ext}, injection SF_{inj}).

Likewise, for each time step j, the resulting equivalent working time wt is

$$wt_j = \frac{E_j}{P_{GSHP}} \tag{16}$$

where P_{GSHP} is the power capacity of the GSHP, at the defined level of the temperature of the end-user (11.43 kW at 35 °C, 10.69 kW at 45 °C and 10.00 kW at 55 °C). By knowing the equivalent working time to
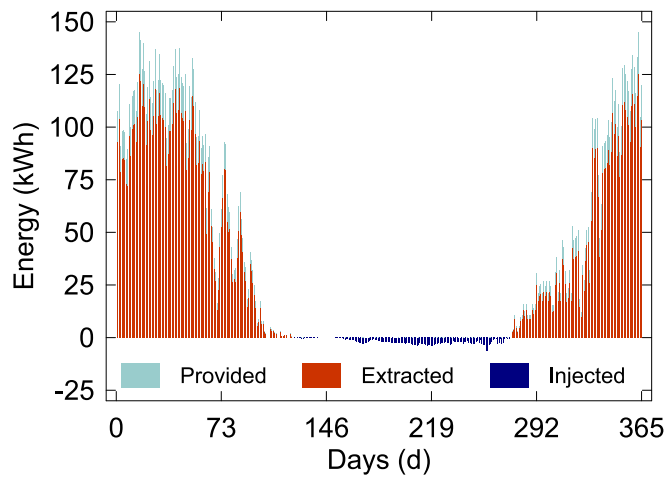
Fig. 10. Extracted and injected energy, with respect to the energy need (distribution and emission system at 35 °C).
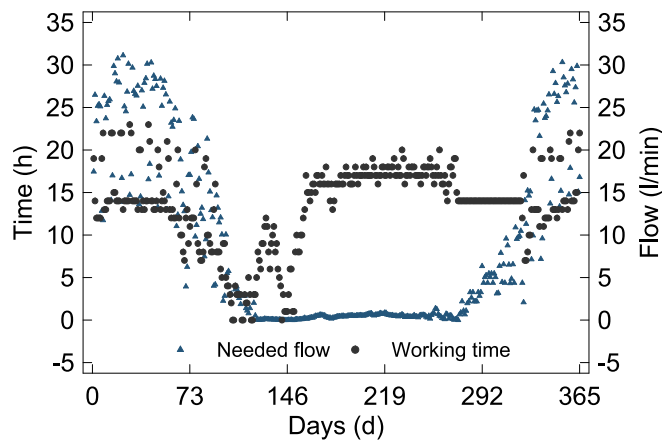

Fig. 11. Working time and circulating flow for the optimum work of the system (distribution and emission system at 35 °C).

Table 22
Seasonal Performance Factor of Smart Flowing heat pump system, considering and not the electric consumption of the driving force.

Mode and distribution temperature	SPF – only heat pump	SPF – heat pump and driving force
Heating – Distribution at 35 °C	6.83	6.46
Heating – Distribution at 45 °C	5.04	4.85
Heating – Distribution at 55 °C	3.70	3.62
Cooling – Distribution at 12 °C	3.04	3.03

satisfy the energy need of each time step, the optimum flow rate can be calculated, and subsequently the head losses of the system and the expected driving force electric consumption (see Section 2.1.2).

At each step of the energy request, according to the efficiency parameters of the chosen GSHP, the following variables were obtained:

- extracted/injected energy to cover the load;
- number of hours of operation per day;
- optimum circulating flow.

The results of the calculation are shown in Fig. 10 in terms of energy exchanged by Smart Flowing according to the energy request and Fig. 11 in terms of working hours per day and correspondent optimum circulating flow.

To obtain the performance of the integrated Smart Flowing – GSHP –

building system, the Seasonal Performance Factor (*SPF*), for both heating (*SPF*$_{heat}$) and cooling (*SPF*$_{cool}$), was calculated. It consists of the ratio between the total energy provided, satisfying the energy need (*E*), and the total electric energy consumption of the heat pump (*L*) in Eq. (17)

$$\begin{cases} SPF_{heat} = \dfrac{\sum E_{heat}}{\sum L_{heat}} \\[2mm] SPF_{cool} = \dfrac{\sum E_{cool}}{\sum L_{cool}} \end{cases} \qquad (17)$$

In order to evaluate the effective and complete performance of the system, the electric consumption of the driving force had also to be added to the energy absorbed by the heat pump. This latter was obtained from the experimental values of the circulation pump (Section 2.1.2), modified according to flow rate variation and then multiplied for the number of hours of operation. Table 22 lists the results of *SPF*, both considering and neglecting the contribution of the driving force.

In conclusion, Smart Flowing is always able to provide the necessary heating (and cooling) to the hypothetical end-user located in the selected climatic area. According to the calculations, peak conditions occur only in few days in January, when 23 h of operation per day are needed, with circulation flow of around 1860 l/h.

4. Discussion

4.1. Sensitivity evaluation to the change of drainage water temperature

The obtained results are highly site-specific and mainly dependant on the drainage water flows and temperature levels. However, the collected data provide preliminary information about the Smart Flowing potential, even when subjected to other boundary conditions. By assuming that the downstream dam can guarantee, in every situation, a complete deposition of sediments and water coverage of the system (even in the occurrence of low or very low drainage water flows), the
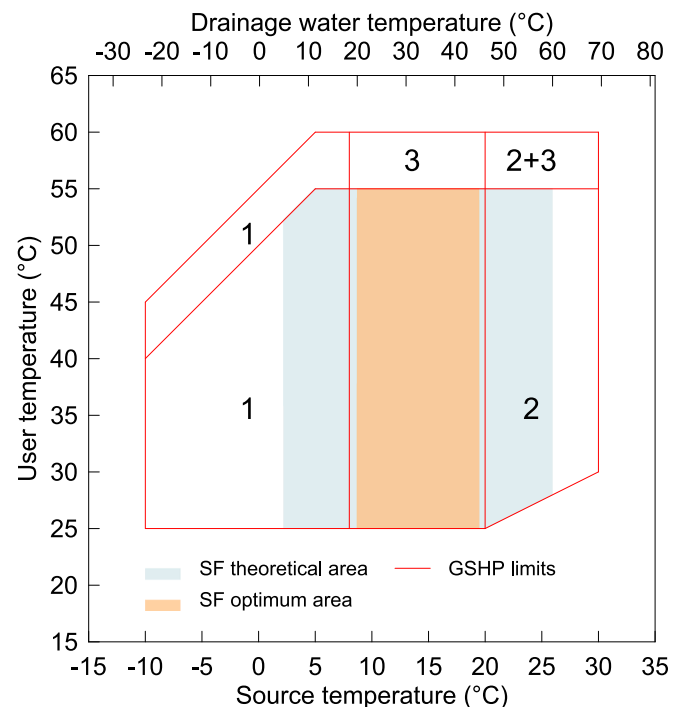

Fig. 12. GSHP limits in working mode. 1: antifreeze needed; 2: control of evaporation; 3: counter-current user side. Blue area: theoretical working zone of Smart Flowing. Orange area: optimum working zone of Smart Flowing (modified from ENEREN, 2021b). (For interpretation of the references to colour in this figure legend, the reader is referred to the web version of this article.)
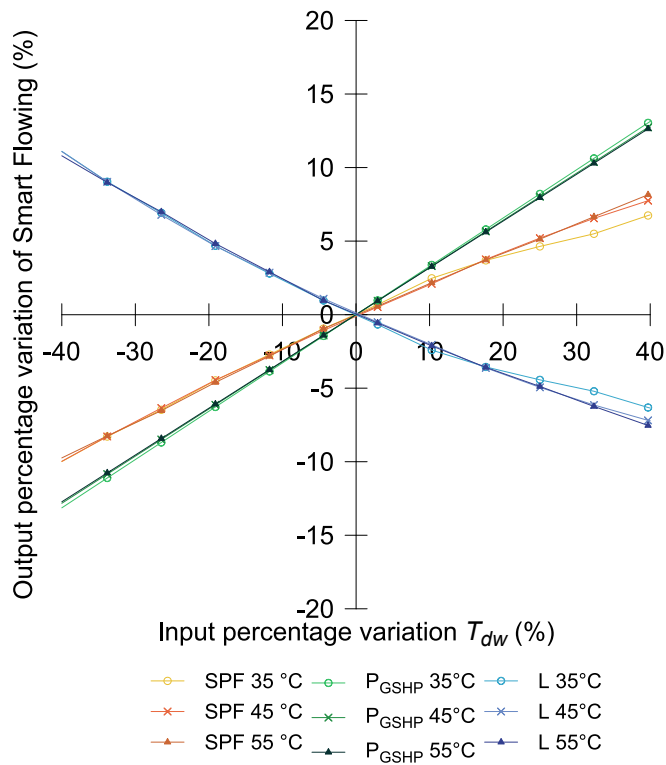
Fig. 13. Sensitivity analysis of the results in terms of power (P_{GSHP}), Seasonal Performance Factor (*SPF*) and electric energy consumption (*L*), with respect to the drainage water temperature variation.

main variable influencing the system operation remains the water temperature level. In order to account for this feature, a sensitivity analysis of the Smart Flowing results was conducted: peak power values of the GSHP machine as well as *SPF* and system electric energy consumption (e.g. the compressor and the driving force) were calculated for a range of possible drainage water temperature levels. As the stabilisation of the circulating temperature in Smart Flowing, $T_{f, stable}$, is strictly related to the drainage water temperature, T_{dw}, during the analyses, the following dependency was found

$$T_{f,stable} = \kappa \cdot T_{dw} \qquad (18)$$

where the factor κ was obtained by applying the direct proportion law between the measured data from the tests ($T_{f,stable} = 13.6$ °C and corresponding $T_{dw} = 31.5$ °C) and it is equal to 2.31.

The sensitivity analyses are bounded by the Smart Flowing working zone, which is based on the GSHP working temperature limits (Fig. 12).

For tunnels operating in different environments, a realistic range of the drainage water temperature could be from 5 °C to 60 °C, which is mirrored by an interval of the possible stationary working fluid of Smart Flowing from 2 °C to 26 °C. In relative percentage terms, with respect to the stationary temperature of the tests (i.e. 13.6 °C), it results in a wide variability range, from −85 % to + 90 %.

According to the technical indication of the selected heat pump (ENEREN, 2021b), when using source fluid temperatures lower than 8 °C, it is advisable to add antifreeze to the liquid. For environmental requirements, the use of this additive should be avoided in Smart Flowing operations, in order to prevent drainage water contamination in case of pipe breakage. Therefore, increasing the minimum fluid working temperature to avoid antifreeze use imposes strong restrictions on the range of application of Smart Flowing, with a minimum drainage water temperature at 20 °C.

Furthermore, an elevated temperature of drainage water needs to be carefully checked, since evaporation control is required when the

working fluid temperature exceeds 20 °C. According to the calculations conducted using Equation (17), this could happen with drainage water temperatures higher than 45 °C.

Due to these two constraints, the optimum operation range of Smart Flowing is expected to be obtained with drainage water temperature values between 20 and 45 °C, reflected in a range of stationary working fluid temperatures between 8.5 and 19.5 °C. It means the range of admissible values falls between −37.5 % and + 43.5 %, with respect to the working conditions of the Smart Flowing prototype considered as 31.5 °C of drainage water temperature and 13.6 °C of working fluid temperature.

Apparently, these conditions reflect most tunnel situations; however, some cases exist where drainage water temperatures were found below 20 °C (Rybach, 2010) or above 45 °C (Hu et al., 2021).

Following this, a detailed sensitivity analysis for three selected end-user temperature levels was performed, i.e. 35 °C, 45 °C and 55 °C. The analysis comprehended, as target variables, the *SPF* in heating mode, the peak power provided (P_{GSHP}) and the total energy consumption (*L*) for one year of operation. The percentage increase or decrease of selected target variables could be identified, for any variation of working conditions with respect to the Smart Flowing prototype results presented in Section 3.3, assumed as origin in Fig. 13.

The sensitivity analysis showed how the results are (directly or inversely) proportional to the drainage water temperature. A 10 % reduction of drainage water temperature with respect to that of the Brenner Base Tunnel case (28 °C versus 31 °C) is expected to cause a performance reduction of the geothermal system of around 2.5 %, which corresponds to an increase in electricity consumption. On the contrary drainage water temperature up to 40 °C (+27 % with respect to the prototype case) should lead to an *SPF* increase of around 5 %.

Following these results, an efficient application of Smart Flowing is considered feasible in several tunnelling conditions, especially if a considerable drainage water flow is expected and underground water temperatures range between 20 and 45 °C. However, each application needs to be carefully investigated for the specific case, considering the effective needs of heating and cooling of the involved area and the practical installation features.

4.2. Economic and practical considerations

The investment costs for Smart Flowing prototype and its testing system were:

- € 1,930.00 for materials and assembly outside the tunnel;
- € 620.00 for assembly inside the tunnel;
- € 6,550.00 for heat pump machine with additional tools and sensors;
- € 3,600.00 for installation and set-up of the heat pump in the tunnel.

Hence, the costs for the implementation of the system prototype (manufacturing and installation) were € 2,550.00, while a further amount of € 10,150.00 was necessary for the testing system.

With an exchange pipe length of 75 m, the specific cost of Smart Flowing was then 34.00 €/m. It is worth noting that the entire system was handcrafted, therefore the adoption of the system on a wider scale should reduce the investment cost (for example of the welded-mesh support, or the steel dam) due to industrialised processes and production lines. Additionally, calculations confirmed that Smart Flowing in extraction mode can provide at least 80 W/m per pipe length and 285 W/m^2 per heat exchange area, quite high values when compared to classical shallow geothermal alternatives (VDI4640:2010; UNI11466:2012; Sanner, 2018). With the exposed values of *SPF* (Table 22), Smart Flowing, if coupled to a GSHP, can provide heating costs reduction from 60 to 80 % (depending on the energy and raw materials costs and end-user alternatives).

For instance, by assuming a price of 2 €/Sm^3 for natural gas as an alternative energy source, 0.4 €/kWh as the price for electric energy and

a full *SPF* of 6.46, the heating cost savings for the model end-user who chooses Smart Flowing are

$$\begin{cases} \text{Cost}_{\text{Natural Gas}} = 14,087\ kWh \div 9.94 \frac{kWh}{Sm^3} \times 95\% \times 2 \frac{\text{€}}{Sm^3} = 2,983\text{€} \\ \text{Cost}_{\text{Smart Flowing}} = 14,087\ kWh \div 6.46 \times 0.4 \frac{\text{€}}{kWh} = 872\text{€} \end{cases} \quad (19)$$

For each year, the costs savings are expected to be more than 2,000 €, corresponding to a 70 % reduction. On account of the potentially huge savings, the return on investment may be relatively swift. In mountain environments, the lack of consumers in the immediate vicinity of tunnel portals, hindering the realization of energy and water networks, should be taken into consideration, as this condition affects not only the exploitation of geothermal energy but also that of fossil fuels, biomass and other alternatives. Due to this issue, the direct use of energy for tunnel purposes, such as tunnel heat dissipation, air conditioning of emergency stations and other purposes should be evaluated case by case. With reference to the BBT system, during its operational phase, the exploratory tunnel is supposed to host technical equipment necessary for the railway lines in the main tunnels and to function as a central drainage system for the entire BBT. Therefore, a potential application of the Smart Flowing prototype to be studied and evaluated could be the air conditioning of control rooms, by dissipating heat directly through the water discharge channel.

5. Conclusions

The paper presented the experimental campaign and modelling of the Smart Flowing prototype, a new type of geothermal heat exchanger placed between the invert upper and lower segments of the BBT exploratory tunnel, where the overburden reaches about 1000 m. Smart Flowing consists of seven modules for a total length of 90 m of absorber pipes, 75 m of which perform the heat exchange with drainage water and the remaining 15 m are used to close the loop and connect the exchanger with the ASHP for testing. The collector was specifically designed to adapt itself to the TBM space limitations and was installed in compliance with the working schedule established at the construction site. The system's major advantage lies in its modular and compact design that has a positive effect on all the activities, in terms of time required to manufacture the system and for the installation sequence, which lasted six hours and a half. In fact, the installation of Smart Flowing does not require modifications to the tunnel lining cross-section.

The experimental and testing work proved the practical feasibility of the Smart Flowing prototype as well as the preliminary technical and economic potential to exploit energy from the drainage water in tunnels, with specific reference to power, temperature levels and efficiency expected.

An empirical thermal model of Smart Flowing was proposed, based on the test results. The model is an adaptation of the formula commonly used for designing shallow horizontal heat exchangers. The equations were duly modified to consider the specific situation at the tunnel site and the contribution given by the water movement. Some correction factors were also introduced, based on the experimental results.

The application of the model, validated against the experimental tests, confirmed that the drainage water flow guarantees the long-term stabilization of circulating water temperature and fast heat recovery when the system is switched off. In the conditions of the BBT exploratory tunnel, Smart Flowing can provide heat for at least 80 W/m of pipe and 285 W/m^2 of exchange area. When connected to a ground source heat pump, thanks to the long-term temperature stabilization the Seasonal Performance Factor of Smart Flowing can exceed values of 5, hardly reachable by standard GSHP systems. Through the use of a sensitivity analysis, the obtained results were generalized, assessing the functioning of Smart Flowing for a drainage water temperature between 20 and 45 °C. The economic value of the system is potentially very high, but

proper utilizations in the context of deep tunnels should be still investigated.

A programme of further experiments dedicated to the further validation of the design procedure and the application to underground utilities is currently underway.

CRediT authorship contribution statement

F. Tinti: Conceptualization, Methodology, Validation, Formal analysis, Writing – original draft, Writing – review & editing. **C. Spaggiari:** Methodology, Investigation, Data curation, Validation, Formal analysis, Writing – original draft, Writing – review & editing. **M. Lanconelli:** Methodology, Investigation, Data curation, Writing – original draft, Writing – review & editing. **A. Voza:** Methodology, Resources, Writing – original draft, Writing – review & editing, Project administration. **D. Boldini:** Supervision, Writing – original draft, Writing – review & editing, Project administration.

Declaration of Competing Interest

The authors declare that they have no known competing financial interests or personal relationships that could have appeared to influence the work reported in this paper.

Data availability

Data will be made available on request.

Acknowledgements

References

Boldini, D., Bruno, R., Egger, H., Stafisso, D., Voza, A., 2018. Statistical and geostatistical analysis of drilling parameters in the Brenner Base tunnel. Rock Mech. Rock Eng. 51 (6), 1955–1963.

Boldini, D., Bruno, R., Tinti, F., Ferrari, M., Kasmaeeyazdi, S. Lanconelli, M., 2016. Possibili impieghi applicativi della risorsa geotermica nell'ambito dei lavori di realizzazione e dell'esercizio della Galleria di Base del Brennero, Technical Report, 20 pp.

Buhmann, P., Moormann, C., Westrich, B., Pralle, N., Friedemann, W., 2016. Tunnel geothermics a German experience with renewable energy concepts in tunnel projects. Geomech. Energy Environ. 8, 1–7. https://doi.org/10.1016/j. gete.2016.10.006. Themed Issue on Selected Papers Symposium of Energy Geotechnics 2015 Part II.

Burger, U., Geisler, T., Lehner, F., Cordes, T., Marcher, T., 2022. Sectional discharges as geothermal potentials of deep tunnels. Geomechanik und Tunnelbau 15 (1), 92–103.

Casale, S., Voza, D., Boldini, D., Bruno, R., Tinti, F., Ferrari, M., Kasmaee, S., 2015. Swiftly Green Best-Practice Case: Infrastructure spatial planning and environmental effects. Swiftly Green European Project. 92.

Chase, D.V., Walsky, M., 2003. Advanced water distribution modeling and management. Haestead Press. ISBN: 0971414122.

Dematteis, A., Gilli, P., Parisi, M.A., Ferreri, L., Furno, F., 2016. Maddalena exploratory adit: feedback on hydrogeological and geothermal aspects. Acque Sotterranee - Italian Journal of Groundwater AS19-201, 35–42. https://doi.org/10.7343/as-2016-201.

Eneren, 2021a. Technical data air/water heat pump. Model NAW006.

Eneren, 2021b. Technical data water/water heat pump. Model GSE006.

Foderà, G.M., Voza, A., Barovero, G., Tinti, F., Boldini, D., 2020. Factors influencing overbreak volumes in drill-and-blast tunnel excavation. A statistical analysis applied to the case study of the Brenner Base Tunnel - BBT. Tunn. and Undergr. Sp. Tech. 103475 https://doi.org/10.1016/j.tust.2020.103475.

Frodl, S., Franzius, J.N. Bartl, T., 2010. Design and construction of the tunnel geothermal system in Jenbach. Geomech. Tun. 2010, 3(5), 658-68. DOI: 10.1002/ geot.201000037.

Geisler, T., Voit, K., Burger, U., Cordes, T., Lehner, F., Götzl, G., Wolf, M., Marcher, T., 2022. Geothermal potential of the Brenner Base Tunnel — Initial evaluations. Processes 10, 972. https://doi.org/10.3390/pr10050972.

Hu, Y., Wang, Q., Wang, M., Liu, D., 2021. A study on the thermo-mechanical properties of shotcrete structure in a tunnel, excavated in granite at nearly 90°C temperature. Tunn. and Undergr. Sp. Tech. 110, 103830 https://doi.org/10.1016/j.tust.2021.103830.

Insana, A., Barla, M., 2020. Experimental and numerical investigations on the energy performance of a thermo-active tunnel. Renew. Energy 152, 781–792. https://doi.org/10.1016/j.renene.2020.01.086.

ISTAT - Italian National Institute of Statistics, 2022. GeoDemo, Inhabitants from the Municipalities of "Fortezza" and "Campo di Trens" https://demo.istat.it/popres/index.php?anno=2022&lingua=ita.

Kasmaee, S., Tinti, F., Ferrari, M., Lanconelli, M., Boldini, D., Bruno, R., Egger, H., di Bella, R., Voza, A., Zurlo, R., 2016. Use of Universal Kriging as a tool to estimate mountain temperature distribution affected by underground infrastructures: the case of the Brenner Base Tunnel. In: European Geothermal Congress - ECG 2016, Strasbourg, 10 pp.

Kostner, A., 2011. The Brenner Base Tunnel (BBT): A source of renewable energy. A survey on the geothermal energy potential of the tunnel water at the BBT's South Portal and its utilization possibilities for district heating purposes, Master Thesis in "Renewable Energy". Technical University of Wien.

Lanconelli, M., 2016. Studio di fattibilità per lo sfruttamento geotermico delle gallerie delle Brennero. Master thesis in Civil Engineering. University of Bologna, Bologna, Italy, p. 216 pp..

Lanconelli, M., Voza, A., Egger, H., Zurlo, R., Boldini, D., Tinti, F., Ferrari, M., Kasmaee, S., 2018. Studio di fattibilità per lo sfruttamento geotermico delle gallerie del Brennero. Gallerie e Grandi Opere in Sotterraneo 126, 35–47.

Meibodi, S.S., Loveridge, F., 2022. The future role of energy geostructures in fifth generation district heating and cooling networks. Energy 240, 122481. https://doi.org/10.1016/j.energy.2021.122481.

Rehau, 2013. System for underfloor heating and cooling, technical information - system guidelines, piping and connection, planning and assembly.

Rybach, L., 2010. Geothermal use of warm tunnel waters: principles and examples from Switzerland. Transactions - Geothermal Resources Council 34 (2).

Rybach, L., 2015. Innovative energy-related use of shallow and deep groundwaters - Examples from China and Switzerland. Central European Geology 58 (1–2), 100–113. https://doi.org/10.1556/24.58.2015.1-2.7.

Rybach, L., Busslinger, A., 2013. Verification of rock temperature prediction along the Gotthard base tunnel - A prospect for coming tunnel projects, World Tunnel Congress 2013 Geneva, 8 pp.

Sanner, B., 2018. Standards and Guidelines for UTES/GSHP wells and boreholes. In: In: 14th International Conference on Energy Storage 25–28 April 2018, p. 19 pp..

Spaggiari, C., 2021. Concept, design, and testing of an innovative geothermal heat exchanger installed at the Brenner Base Tunnel. University of Bologna, Bologna, Italy, p. 210 pp.. Master thesis in Civil Engineering.

Spaggiari, C., Tinti, F., Lanconelli, M., Voza, A., Boldini, D., 2022. Concept, design and testing of an innovative geothermal heat exchanger installed at the Brenner Base Tunnel, Gallerie e Grandi Opere Sotterranee, 141, 27-41, ISSN: 0393-1641.

Stemmle, R., Menberg, K., Rybach, L., Blum, P., 2022. Tunnel Geothermics - A Review. Geomechanik und Tunnelbaum 15 (1), 104–111.

Tinti, F., Boldini, D., Ferrari, M., Lanconelli, M., Kasmaee, S., Bruno, R., Egger, H., Voza, A., Zurlo, R., 2017. Exploitation of geothermal energy using tunnel lining technology in a mountain environment. A feasibility study for the Brenner Base tunnel - BBT. Tunn. Undergr. Sp. Tech. 70, 182–203. https://doi.org/10.1016/j.tust.2017.07.011.

UNI - Italian National Unification, 2012. UNI11466: Heat Pump geothermal systems - Design and sizing requirements (Sistemi geotermici a pompa di calore - Requisiti per il dimensionamento e la progettazione) https://store.uni.com/uni-11466-2012.

VDI -Verein Deutscher Ingenieure e.v, 2010. VDI4640: Thermal use of underground - Fundamentals, approvals, environmental aspects. The Association of German Engineers.

Voza, A., Valguarnera, L., Marrazzo, L., Ascari, G., Boldini, D., 2022. A new in situ test for the assessment of the rock-burst alarm threshold during tunnelling. Rock Mech Rock Eng. https://doi.org/10.1007/s00603-022-03152-8.

Wilhelm, J., Rybach, L., 2003.Geothermal energy from the tunnels in the Swiss Alps, Technical Report, ENET-230072, 8 pp.